International Journal of Nanomedicine

Dovepress
Taylor & Francis Group

Open Access Full Text Article

ORIGINAL RESEARCH

# Dual-Mode Treatment of Hepatocellular Carcinoma Using RGD Cyclopeptide-Modified Liposomes Loaded with Ce6/DOX

Wentao Xu[1,2,*], Jiajia Zheng[1,2,*], Jiaqi Zhang[1,*], Houhui Shi[3,*], Weili Peng[1], Yang Liu[4], Guodong Feng[5], Yuguang Wang[2], Yi-Jun Liang[6], Jun Chen[1]

[1]Cancer Center, Department of Interventional Medicine, Zhejiang Provincial People's Hospital (Affiliated People's Hospital), Hangzhou Medical College, Hangzhou, 310014, People's Republic of China; [2]College of Biotechnology and Bioengineering, Zhejiang University of Technology, Hangzhou, 310032, People's Republic of China; [3]College of Pharmaceutical Science, Zhejiang University of Technology, Hangzhou, 310014, People's Republic of China; [4]Cancer Center, Department of Ultrasound Medicine, Zhejiang Provincial People's Hospital (Affiliated People's Hospital), Hangzhou Medical College, Hangzhou, Zhejiang, 310014, People's Republic of China; [5]Department of Radiology, Minhang Hospital, Fudan University, Shanghai, People's Republic of China; [6]School of Medicine & School of Mechatronic Engineering and Automation, Foshan University, Foshan, People's Republic of China

*These authors contributed equally to this work

Correspondence: Jun Chen; Yi-Jun Liang, Email chenjun@hmc.edu.cn; liangyijun@fosu.edu.cn

**Background:** Liver cancer is one of the most prevalent cancers globally, with approximately 90% of primary liver cancers being hepatocellular carcinomas (HCC). However, current systemic treatment options (whether monotherapy or combination therapy) are limited and offer only modest survival benefits. The effectiveness of a drug is largely determined by its concentration at the target site. Therefore, an effective drug delivery system must enhance drug accumulation at the target site, enable selective drug release there, and facilitate escape from lysosomes.

**Methods:** cRGD-Lipo@Ce6/DOX was prepared by modifying c(RGDyK) onto the surface of drug-loaded liposomes containing Chlorin e6 (Ce6) and doxorubicin (DOX) through an amide reaction. The targeting capability and uptake mechanism of cRGD-Lipo @Ce6/DOX for HCC were analyzed using flow cytometry. To investigate drug release mechanisms and changes in subcellular distribution following ultrasound stimulation, further studies were conducted. The therapeutic efficacy and biosafety of this dual-modality therapy were then evaluated in an HCC subcutaneous tumor-bearing mouse model.

**Results:** The prepared nanocomplex exhibits a surface charge of −9.91 ± 2.94 mV and an apparent size of 118.07 ± 1.46 nm. Modification of the RGD cyclic peptide on the surface of the drug-carrying liposomes enhanced the targeting and penetration efficiency for HCC. In vitro experiments on drug uptake mechanisms and release demonstrated that reactive oxygen species (ROS) generated by sonodynamic therapy (SDT) promote effective drug release from the carrier into the non-lysosomal region. The combined SDT and chemotherapy treatment achieved a 94% tumor inhibition rate and showed excellent biosafety in HCC subcutaneous tumor-bearing mice.

**Conclusion:** Therefore, the effectiveness of the combination treatment strategy utilizing SDT in conjunction with chemotherapy provides additional treatment options for patients with HCC.

**Keywords:** hepatocellular carcinomas, sonodynamic therapy, dual-modality therapy, lysosomal escape

## Introduction

Hepatocellular carcinoma (HCC) represents 80% of all primary liver cancers worldwide and is the sixth most common cancer and the third leading cause of cancer-related deaths.[1] Due to the typically late appearance of symptoms, more than half of HCC cases are diagnosed at an advanced stage, often necessitating systemic treatment.[2,3] In the past, doxorubicin (DOX) was a primary first-line anticancer drug for various cancers, including advanced HCC. However, its efficacy was severely limited due to drug resistance and significant cardiotoxicity.[4] The FDA's approval of sorafenib as a first-line treatment for advanced HCC in 2007 dramatically altered treatment paradigms, yet it only provides a modest survival

Received: 26 December 2024
Accepted: 15 March 2025
Published: 27 March 2025

benefit of about 2.8 months.[5] More recently, the combination of immune checkpoint blockade (ICB) has improved the prognosis for patients with advanced HCC. Nonetheless, this combination therapy achieved only a 30% objective response rate (ORR) and a modest survival extension of 5.8 months.[6,7] Moreover, the incidence of adverse events associated with combination therapy remains a concern that needs improvement.[8] For patients with advanced HCC who had previously been treated and had disease progression, suboptimal therapies were considered, but these resulted in less than 3 months of remission in overall survival compared to placebo.[9,10] Therefore, there is an urgent need for new treatment strategies. In recent years, sonodynamic therapy (SDT) offers a non-invasive treatment option with precise spatiotemporal control and minimal systemic toxicity, making it a potential candidate for combination therapy.[11] However, simply mixing different therapeutic drugs to treat cancer may not achieve the desired therapeutic effect, given the random release behavior of these drugs in the body and varying tumor uptake.

To enhance the accumulation of combination drugs at the target site, active targeting can be achieved by modifying the surface of nanoparticles with polypeptides, antibodies, or nucleic acid aptamers, which mediate receptor-ligand interactions to enrich drugs specifically in tumor cells. For example, the RGD peptide, a short tripeptide, selectively binds to αvβ3 integrin, which is overexpressed on tumor cell membranes but not on normal hepatocytes.[12–14] In a demonstration, Yang et al developed 2D $Ti_3C_2$ nanosheets coated with thin-shell silica and modified with RGD ($Ti_3C_2$@mMSNs-RGD) on the surface. Compared to unmodified $Ti_3C_2$@mMSNs, the RGD-modified nanoparticles showed a 5.59% increase in targeting efficiency to HCC tissues.[15]

To improve the controllable release of drugs within the body, intelligent drug delivery systems (IDDS) that respond to various stimuli have been extensively investigated for the treatment of multiple cancers. These stimuli include both internal stimuli (such as pH, enzymes, and redox, etc). and external stimuli (light, ultrasound (US), and magnetic fields, etc). Among these, ultrasound-controlled IDDS holds significant promise for achieving targeted drug release. Compared to other stimulus-responsive systems, US-controlled IDDS may be more suitable for in vivo applications due to its non-invasiveness, non-ionizing radiation, high tissue penetration depth, and spatiotemporal controllability.[16] Additionally, it is often overlooked that the release of drugs into the cytoplasm is significantly restricted. Most DDSs are internalized by cells through clathrin-mediated endocytosis (CME), leading to drug degradation in lysosomes and subsequent exocytosis from the cell.[17] Research has shown that US can induce effects similar to photochemical internalization (PCI), aiding in drug escape from lysosomes.[18]

Lipid nanoparticles (LNPs) were among the first nanocarriers approved by the FDA for clinical use, and they have been extensively developed and widely applied. This is largely due to their inherent biocompatibility, ease of synthesis, and scalability. However, their clinical application has been limited by two key challenges: the lack of efficient lysosomal escape and the tendency for random drug release.[19,20] This study investigates the use of US-activated liposomes to facilitate drug release at tumor sites and enhance the ability of chemotherapeutic drugs to penetrate tumor nuclei. Moreover, the reactive oxygen species (ROS) generated by SDT can further eliminate tumor cells. Herein, we incorporated DOX and the sonosensitizer Chlorin e6 (Ce6) into liposomes to construct a cooperative DDS. As illustrated in Scheme 1, targeting with the c(RGDyK) cyclic peptide and US-activated Ce6 produced ROS that disrupted the liposomes, ensuring precise drug release at the target site. Ultrasound stimulates Ce6 to generate ROS and disrupt the endosome, allowing DOX to pass through intracellular barriers and act more effectively as a chemotherapy agent. The synergy and high bioavailability of these components offer additional opportunities for the development of new combination therapies for HCC.

# Materials and Methods

## Materials

Amino-Phalloidin and 4.6-diamino-2-phenylindole (DAPI) were both acquired from Yeasen Biotech Co., Ltd. (Shanghai, China). LysoTracker Green (Red), cell trackers (Dil) and DCFH-DA were obtained from Beyotime Biotechnology (Shanghai, China). Tris(2-carboxyethyl) phosphine (TCEP), penicillin-streptomycin, trypsin-EDTA, fetal bovine serum (FBS), and phosphate-buffered saline (PBS, pH=7.4) were supplied by Thermo Fisher Scientific in Waltham, MA, USA. The Cell Count Kit-8 (CCK8) was purchased from LABLEAD.Inc. (Beijing, China). Cell apoptosis kit and cell cycle kit

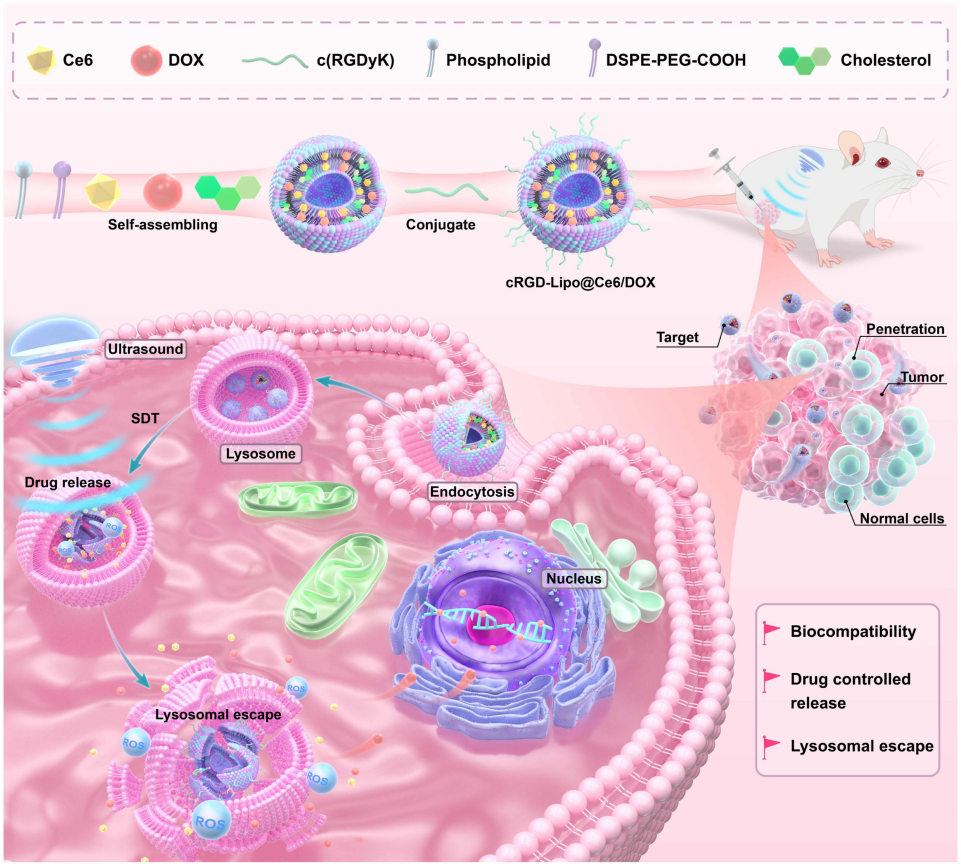


**Scheme 1** The drug accumulates in the tumor area through intratumoral injection and specific binding of the RGD cyclic peptide to tumor cell surface receptors; After endocytosis of the drug into the cells, the sonosensitizer is stimulated by US to produce ROS, which leads to lysosomal escape and allows DOX to diffuse into the nucleus.

were supplied by MULTI SCIENCES (Hangzhou, China). High glucose DMEM was sourced from VivaCell (Shanghai, China). Hoechst 33342, filipin, and chlorpromazine were acquired from MedChemExpress (New Jersey, USA). MES buffer (0.05 M, pH 6.7), 1-(3-dimethylaminopropyl)-3-ethylcarbodiimide hydrochloride (EDC), N-hydroxysuccinimide (NHS), and Maleimide-PEG2000-amine (Mal-PEG2000-$NH_2$) were obtained from Aladdin Biochemical Technology Co., Ltd., (Shanghai, China). C(RGDyK) was acquired from GL Biochem Ltd., (Shanghai, China).

## Preparation of cRGD-Lipo@Ce6/DOX

The drug-carrying liposomes were purchased from Nanjing Dongna Biotechnology Co., LTD., and obtained technical support. The formulation of Lipo@Ce6/DOX is accomplished through the thin film dispersion technique, wherein it is compounded to encapsulate 100 milligrams of lecithin, 13 milligrams of cholesterol, and 13 milligrams of DSPE-mPEG2000 (Aladdin Biochemical Technology Co., Ltd., Shanghai, China). The liposomes, designed to carry the therapeutic agents, are derived from a mixture of 10 milligrams of Ce6 and 2.4 milligrams of adriamycin in chloroform, subsequent to a series of meticulous processes including vacuum extraction, evaporation of the volatile solvent, hydration, US dispersion, and mechanical disruption.

Lipo@Ce6/DOX was added to MES buffer (0.05 M, pH 6.7) containing 0.1 M EDC, 5 mm NHS, and Mal-PEG2000-$NH_2$. The mixture was stirred at room temperature for 2 hours. The resulting solution was then subjected to ultrafiltration (MWCO: 30,000 Da) at 800 xg for 15 minutes. Pre-TCEP-mixed cRGD was added to the purified solution and stirred at room temperature for an additional 2 hours. The solution underwent another round of ultrafiltration, and the final purified liquid was stored at 4 °C.

To determine the solid weight of Lipo@Ce6/DOX, 1 mL of the sample was added to a centrifuge tube, and the solid weight was calculated using the drying differential weight method. The sample was then dissolved in 1 mL of methanol. The


https://doi.org/10.2147/IJN.S509387

absorption values were measured at wavelengths of 503 nm and 669 nm, respectively. The Ce6 and DOX loading content was subsequently calculated based on the standard curve. The loading content of Ce6 (DOX) was subsequently calculated based on the standard curve. The encapsulation efficiency and loading efficiency were determined using the following formulas: encapsulation efficiency = $W_{loading\ drug} \times W_{drug}^{-1} \times 100\%$; loading efficiency = $W_{loading\ drug} \times W_{Lipo@Ce6/DOX}^{-1} \times 100\%$. The encapsulation efficiency and loading efficiency of Ce6 and DOX were found to be 99.16% (w/w) and 99.53% (w/w), respectively. The loading efficiency of Ce6 and DOX were found to be and 8.9% (w/w) and 2.35% (w/w), respectively.

To obtain pure cRGD-Lipo (DiI)@Ce6, 5 μM DiI was mixed with cRGD-Lipo@Ce6 and incubated at 37 °C for 0.5 hours. The mixture was then subjected to ultrafiltration, repeated three times.

## Characterization of Nanocomplexes

The size and zeta potential were measured using a Zetasizer (Malvern Zetasizer; Malvern Instruments Ltd., Malvern, UK). The ultraviolet-NIR absorption spectrum was obtained with a UV-Visible Spectrophotometer (Thermo Fisher, EVOLUTION220, USA). The morphologies were observed using a transmission electron microscope (TEM, FE, JEM-F200, Japan).

To investigate the stability of the cRGD-Lipo@Ce6/DOX in different pH environments, 100 μL of the aqueous solution of the material (1 mg $mL^{-1}$) was diluted to 3 mL with buffers of varying pH and stored at 4 °C. The hydrated particle size and PDI were characterized using a Zetasizer.

## Drug Release

1.5 mL of cRGD-Lipo@Ce6/DOX was added to a dialysis bag (MWCO: 35,000 Da) and placed in a 500 mL beaker containing PBS. The released liquid was collected regularly and analyzed using a UV-visible spectrophotometer. Before the dialysis experiment, cRGD-Lipo@Ce6/DOX was pretreated with an ultrasonic exciter at 80% amplitude and a frequency of 1.0 MHz for 5 minutes. The dialysis and measurement steps were then repeated.

## Cells and Tumor Spheroids Culture

HHL-5, Huh 7, and Hep G2 cells were cultured in DMEM and MEM supplemented with 10% fetal bovine serum and 1% penicillin/streptomycin. The cells were maintained at 37 °C in a humidified atmosphere with 5% $CO_2$. HHL-5 cells represent human hepatocytes, while Hep G2 and Huh 7 cells are HCC cells. The cell lines were sourced from the National Certified Cell Culture Collection in China.

To generate tumor spheroids, Huh 7 cells (at a density of $1\times10^6$ cells $mL^{-1}$) were suspended in fresh DMEM containing 0.12% (w/v) methylcellulose. The cell suspension was evenly distributed onto the surface of a cell culture dish, and 8 mL of PBS was added. After 48 hours, the compact spheres were transferred individually to low-adhesion 96-well plates and incubated for an additional 48 hours.

## HCC Targeting Efficiency

HHL-5, Huh 7, and Hep G2 cells were seeded in 24-well plates at a density of $1.5\times10^5$ cells $well^{-1}$ and incubated for 12 hours. The culture medium was then replaced with fresh medium containing a specified amount of Free Ce6 (2 μg $mL^{-1}$) or cRGD-Lipo@Ce6 (2 μg $mL^{-1}$ Ce6), and the cells were incubated for an additional 12 hours. After incubation, the cells were washed three times with PBS and analyzed using flow cytometry (Beckman Coulter, Navios, USA).

## Tumor Spheroids Penetration

Multicellular spheroids (MCSs) were extracted and transferred to a 24-well low-adhesion plate. The spheres were washed three times with PBS and then treated with culture medium containing free Ce6, Lipo@Ce6, and cRGD-Lipo@Ce6 (each at a Ce6 concentration of 4 μg $mL^{-1}$) for 12 hours, respectively. After treatment, the MCSs were washed three times with PBS, transferred to confocal dishes, and observed using fluorescence excitation confocal microscopy through the Cy5 fluorescence channel.

## Endocytosis Mechanism of NPs

The uptake of cRGD-Lipo@Ce6 by Hep G2 and Huh 7 cells was analyzed using flow cytometry. Cells were seeded at a density of $1.5\times10^5$ cells well$^{-1}$ in 24-well plates and incubated for 24 hours. They were then treated with various inhibitors and maintained at a low temperature (4 °C). After washing twice with PBS, the cells were exposed to cRGD-Lipo@Ce6 and incubated for 1 hour. Following incubation, the cells were washed twice with PBS, trypsinized, and centrifuged at 300 xg for 3 minutes to remove the trypsin. The resulting cell pellets were resuspended in PBS and analyzed by flow cytometry.

For each inhibitor (filipin at 7.5 μM, chlorpromazine at 30 μM, and ethyl isopropyl amiloride at 20 μM), Hep G2 and Huh 7 cells were pretreated with the inhibitor for 1 hour.

## Lysosome Escape

Intracellular drug release mechanism of cRGD-Lipo@Ce6/DOX in lysosomes was observed using a Confocal Laser Scanning Microscope (CLSM, Leica TCS SP5 Confocal, LEICA Inc., California, USA). Hep G2 and Huh 7 cells were seeded in small dishes at a density of $1.5\times10^5$ cells well$^{-1}$ and incubated for 24 hours. cRGD-Lipo (DiI)@Ce6 was then added, and the cells were incubated for 2, 6 and 12 hours, respectively. After incubation, cells were stained with LysoTracker Green DND-26 and Hoechst 33342 before being analyzed by CLSM.

Intracellular localization following endocytosis was observed using a Confocal Laser Scanning Microscope. Hep G2 and Huh 7 cells were seeded in small dishes at a density of $1.5\times10^5$ cells well$^{-1}$ and incubated for 24 hours. cRGD-Lipo @Ce6 was then added, and the cells were incubated for 1, 3 and 6 hours, respectively. In the other group, US stimulation was applied. After incubation, cells were stained with LysoTracker Green DND-26 and Hoechst 33342 before being analyzed by CLSM.

The change in LAMP1 content after US stimulation was observed using a Leica TCS SP5 Confocal Laser Scanning Microscope. Hep G2 cells were seeded in small dishes at a density of $1.5\times10^5$ cells well$^{-1}$ and incubated for 24 hours. cRGD-Lipo@Ce6 was then added and incubated for 2 hours. Following incubation, the cells underwent US stimulation (80% duty cycle, 3 min) and continue incubation 6 hours. The cells were then fixed with 4% paraformaldehyde for 30 minutes, permeabilized with 0.3% Triton X-100, and blocked with 5% skim milk. Primary antibodies (LAMP 1, Abcam, ab24170) were incubated at 4 °C overnight, followed by incubation with secondary antibodies for 1 hours. After washing, cells were stained with DAPI, and analyzed by CLSM.

## ROS Generation

Hep G2 cells were seeded in 24-well plates at a density of $1.5\times10^5$ cells well$^{-1}$ and incubated for 12 hours. The cells were treated with PBS, Free Ce6, or cRGD-Lipo@Ce6 for 8 hours. After treatment, the cells were washed twice with PBS. Ultrasound (US; 1.0 MHz, 80% duty cycle) was applied for 5 minutes. Following this, the cells were harvested and stained with DCFH-DA, and then analyzed using flow cytometry.

## In Vitro Antitumor Treatment

Hep G2 and Huh 7 cells were seeded in 24-well plates at a density of $1.5\times10^5$ cells well$^{-1}$ and incubated for 12 hours. The cells were treated with Free Ce6, Lipo@Ce6, cRGD-Lipo@Ce6, or cRGD-Lipo@Ce6/DOX for 8 hours. After treatment, the cells were washed twice with PBS. Ultrasound (US; 1.0 MHz, 80% duty cycle) was applied for 5 minutes, followed by a 12-hour incubation period. Subsequently, the cells were harvested and stained with annexin V-FITC and PI using the cell apoptosis kit, or with a cell cycle kit, before flow cytometry analysis.

## Animal Study

*General information*: All animal treatment protocols were approved by the Experimental Animal Management Committee of Zhejiang Provincial People' s Hospital (2024061423152047989 2), and all procedures were conducted in strict accordance with their guidelines. Female BALB/c nude mice, aged six weeks, were subcutaneously inoculated with approximately $2.0\times10^6$ Huh 7 cells to establish xenograft tumor models.

*Biodistribution study*. To study the effect of RGD peptide modification on drug delivery efficiency, the Tumor-bearing mice were intratumoral injected 25 μL of Lipo@Ce6/DOX and cRGD-Lipo@Ce6/DOX intratumorally at a dose of 10 mg $kg^{-1}$ Ce6 and 6.4 mg $kg^{-1}$ DOX. Six hours post-injection, the tumors were imaged using the IVIS Spectrum system with the Cy5 fluorescence channel. To study the biological distribution of the drug in mice after injection, the Huh 7 tumor-bearing mice were then randomly assigned to four groups. They were injected with 40 μL of cRGD-Lipo@Ce6/DOX (10 mg $kg^{-1}$ Ce6 and 6.4 mg $kg^{-1}$ DOX). At the specified time points (0 hours, 6 hours, 12 hours, and 24 hours), various organs (heart, liver, spleen, lung, kidney) as well as the tumors were imaged using the IVIS Spectrum system with the Cy5 fluorescence channel.

*Antitumor effect studies in tumor-bearing mice*. The Huh 7 tumor-bearing mice were then randomly assigned to seven groups: PBS, cRGD-Lipo@Ce6 (10 mg $kg^{-1}$ Ce6), cRGD-Lipo@Ce6 + US, cRGD-Lipo@Ce6/DOX (10 mg $kg^{-1}$ Ce6 and 6.4 mg $kg^{-1}$ DOX), DOX (6.4 mg $kg^{-1}$), and cRGD-Lipo@Ce6/DOX + US. Each group received intratumoral injections of 40 μL of the respective drug, followed by US stimulation at 6-hour intervals (1.0 MHz, 80% duty cycle, 5 minutes). Body weight and tumor dimensions were measured every other day, and tumor volume was calculated using the formula V [$mm^3$] = 1/2 × (length [mm] × $width^2$ [$mm^2$]). After 14 days of treatment, major organs were harvested for examination, subjected to H&E staining, and serum samples were collected for biochemical analysis. The tumors were also excised and their size and weight were documented. And tumor inhibition rate was calculated using the formula: tumor inhibition rate = $(W_{control} - W_{treatment}) \times W_{control}^{-1} \times 100\%$.

For histological analysis, internal organs were collected from mice in each group and immediately fixed in 4% paraformaldehyde. The tissues were then dehydrated and embedded in paraffin. Sections were cut at a thickness of 5 μm and stained with H&E to visualize cellular and tissue structures. The stained sections were observed under a light microscope to assess tissue morphology and identify any pathological changes.

## Statistical Analysis

Data are expressed as mean ± standard deviation (SD). Statistical significance was determined using one-way ANOVA analysis. A two-tailed p-value < 0.05 was considered statistically significant. Significance levels were denoted as follows: $*p < 0.05$; $**p < 0.01$; $***p < 0.001$; $****p < 0.0001$. All data were analyzed using GraphPad Prism 9.0 (GraphPad Software, CA, USA).

# Results and Discussion

## Physicochemical Properties

The UV-VIS spectra of Lipo@Ce6/DOX show absorption peaks at 503 nm and 669 nm, which are attributed to the redshift of the internally encapsulated DOX (480 nm) and Ce6 (639 nm), respectively. While no UV absorption was observed in the blank liposomes (Supplementary Figure 1). This effect may be attributed to the close packing of drugs within the liposome, which alters the extent of molecular conjugation and results in a redshift of the UV absorption peak. These results confirmed the successful preparation of the Lipo@Ce6/DOX drug carrier system.

The morphology of the re-dyed cRGD-Lipo@Ce6/DOX was examined using TEM. The hydrated particle size of Lipo@Ce6/DOX was measured to be 98.72 ± 0.69 nm, and the size of the surface-modified RGD cyclopeptide nanoparticles was 118.07 ± 1.46 nm, which was consistent with TEM observations. The zeta potential was −9.91 ± 2.94 mV, an increase from the original −21.83 ± 0.42 mV (Figure 1A-C). The larger size is attributed to the thickness of the hydration layer produced by PEG2000 modification. The reduction in apparent charge may be due to the shielding effect of the PEG layer and the positive charge contributed by the modified RGD cyclic peptide. cRGD -Lipo@Ce6/DOX exhibit excellent stability in buffers of different pH values (Supplementary Figure 2). Specifically, in a neutral buffer at pH 7.4, they maintain good dispersion for the first five days. However, in high-dilution acidic buffers, protonation of fatty acids weakens electrostatic repulsion, leading to an earlier increase in PDI and size (Day 4).[21] The effect of ultrasonic stimulation on drug release in vitro was further investigated using dialysis. After treatment with US, Ce6 and DOX in cRGD-Lipo@Ce6/DOX exhibited an explosive drug release within 1–2 hours (Figure 1D). In the subsequent 5 hours, the drug release continued at a steady rate, which may be attributed to the short lifespan of ROS.

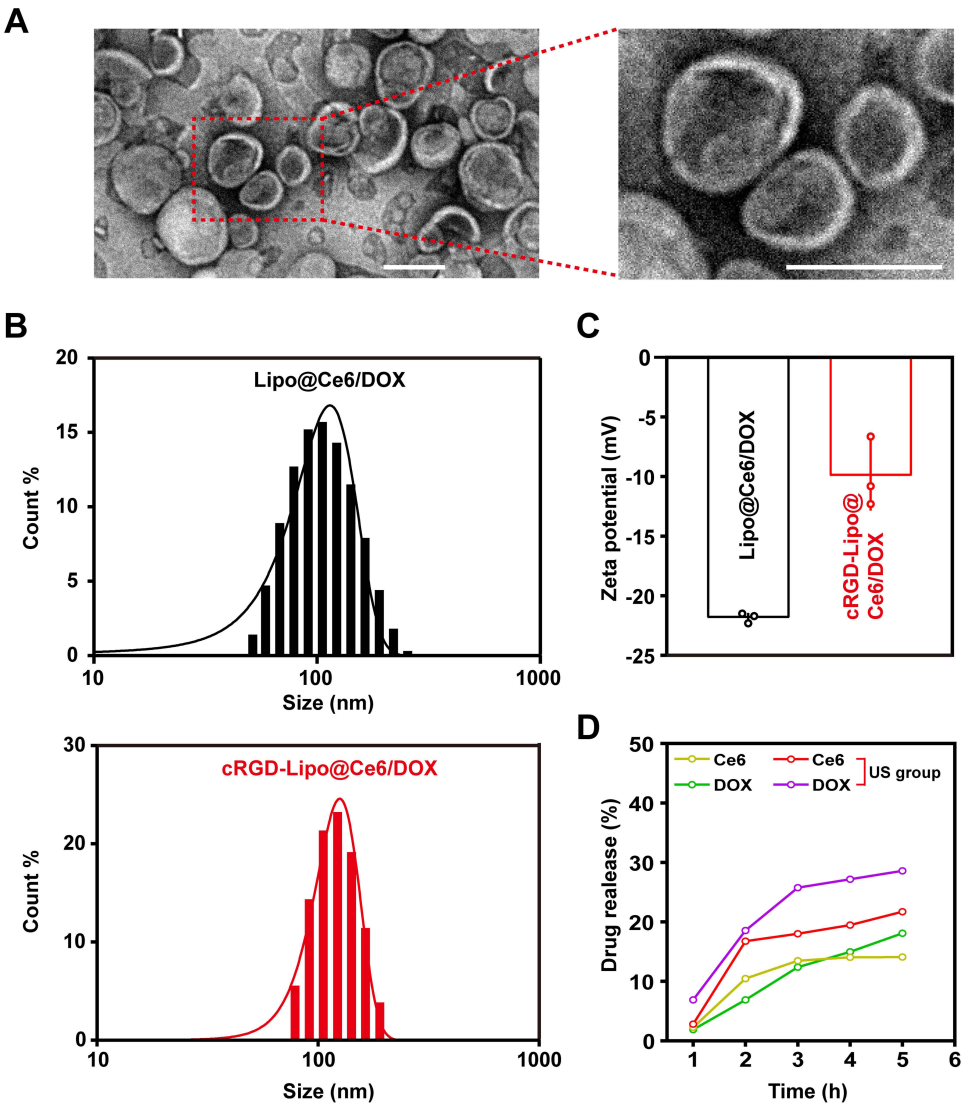


**Figure 1** Characterization of cRGD-Lipo@Ce6/DOX. (**A**) TEM images of cRGD-Lipo@Ce6/DOX, Scale bar: 100 nm. (**B**) Size of Lipo@Ce6/DOX and cRGD-Lipo@Ce6/DOX. (**C**) Zeta potential of Lipo@Ce6/DOX and cRGD-Lipo@Ce6/DOX. (**D**) The release profiles of Ce6 and DOX from cRGD-Lipo@Ce6/DOX were evaluated following different treatments, including the US treatment group and the non-ultrasonic treatment group. US conditions: 80% duty cycle, 5 minutes.

## HCC Targeting Efficiency and Tumor Spheroids Penetration

Fluorescent Ce6 and DOX are securely encapsulated within the LNPs, ensuring identical cell distribution for both drugs (Supplementary Figure 3A and B). To track the internalization of these nanoparticles, we used Ce6 fluorescence in CLSM and flow cytometry with Hep G2 cells. The data showed that the uptake of cRGD-Lipo@Ce6/DOX by Hep G2 cells increased over time (Figure 2A). Additionally, we assessed the targeting ability of the nanoparticles using HHL-5 cells, a human hepatocyte, alongside two HCC cell lines, Hep G2 and Huh 7, via flow cytometry. The fluorescence intensity in the two HCC cell lines was 1.52 and 1.65 times higher than in HHL-5 cells, respectively (Figure 2B). This increased fluorescence intensity likely results from the cRGD peptides on the surface of the nanoparticles specifically targeting integrins that are overexpressed on HCC.[13,22]

The permeability of nanoparticles is influenced by their physical and chemical characteristics. Many researches indicate that anionic nanoparticles exhibit a higher diffusion coefficient in the extracellular matrix compared to cationic nanoparticles.[23] MCSs are utilized as three-dimensional tumor models in vitro to assess drug penetration levels.[24,25] We examined the penetration of cRGD-Lipo@Ce6 in MCSs constructed from Huh 7 cells. Compared to free Ce6, Lipo@Ce6 showed significantly enhanced fluorescence intensity within the spheroids. Notably, the fluorescence of cRGD-Lipo


https://doi.org/10.2147/IJN.S509387

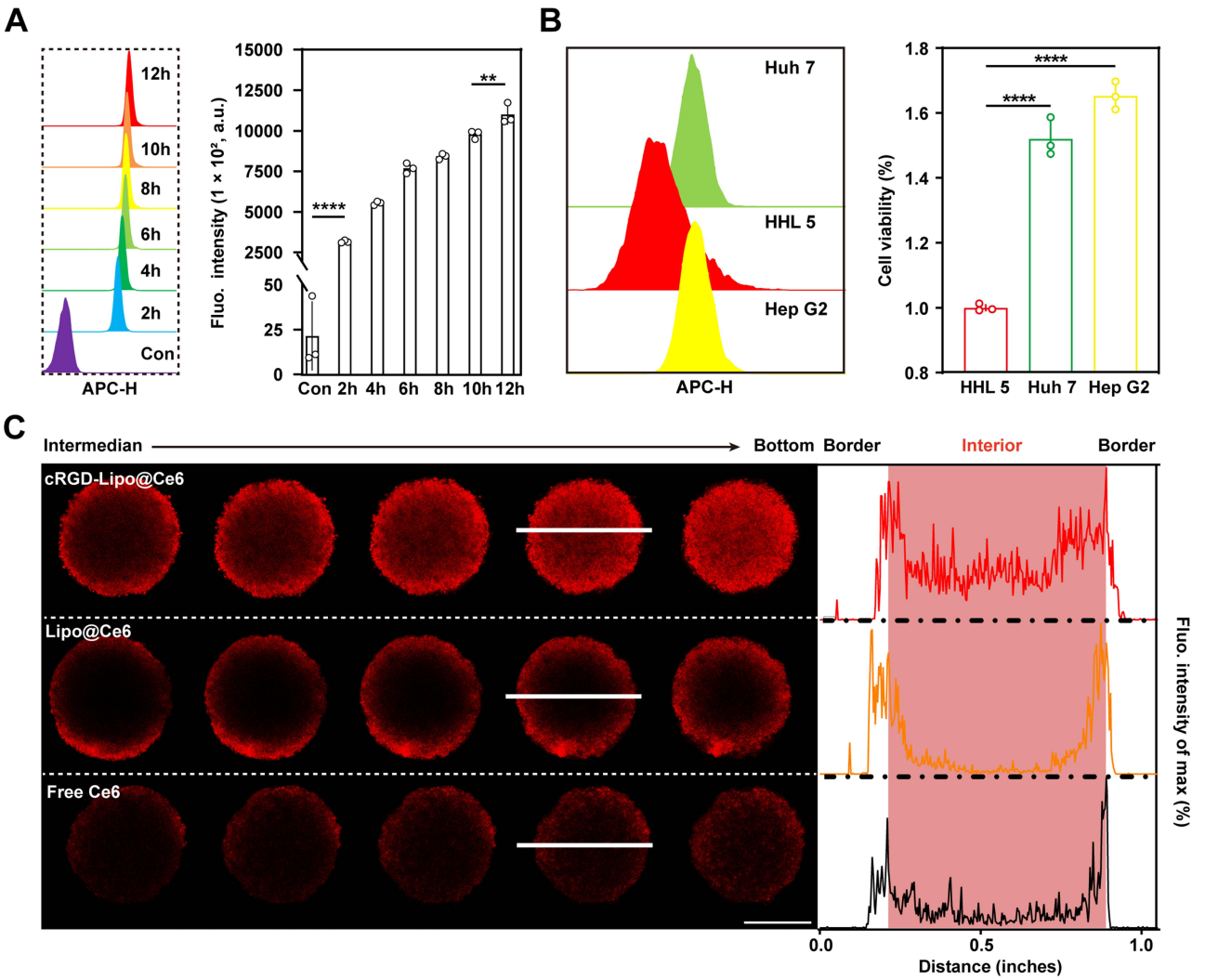


**Figure 2** cRGD-Lipo@Ce6 cell uptake and MCSs penetration. (**A**) Continuous endocytosis of cRGD-Lipo@Ce6 in Hep G2 cells over 12 hours was monitored by flow cytometry using the APC fluorescence channel. cRGD-Lipo@Ce6 (2 μg $mL^{-1}$ Ce6). $^{**}p < 0.01$ and $^{****}p < 0.0001$. (**B**) Flow cytometry analysis of APC fluorescence channels showing uptake of cRGD-Lipo@Ce6 by HHL-5, Huh 7, and Hep G2 cells after a 12-hour incubation with cRGD-Lipo@Ce6 (2 μg $mL^{-1}$ Ce6). $^{****}p < 0.0001$. (**C**) CLSM images showing the distribution of Ce6 in Huh 7 MCSs after a 12-hour incubation with cRGD-Lipo@Ce6 (4 μg $mL^{-1}$ Ce6), Lipo@Ce6 (4 μg $mL^{-1}$ Ce6), or Free Ce6 (4 μg $mL^{-1}$ Ce6). The images show slices from the middle to the bottom of the sphere, with Z-stack scans at 15 μm intervals (left). Fluorescence intensity of the Cy5 fluorescence channel along the white line in a multicellular sphere was analyzed using ImageJ (right). Scale bar: 200 μm.

@Ce6 was detected both outside and inside the spheroids (Figure 2C). This improved distribution is likely due to the rapid diffusion of anionic particles within the matrix and the strong affinity of surface-modified RGD peptides for integrin αvβ3. This interaction disrupts cell adhesion to extracellular matrix proteins, thereby enhancing the delivery of Ce6/DOX.[26]

## SDT Improved Subcellular Distribution

Receptor-mediated endocytosis is the primary mechanism for drug uptake into cells.[27] Initially, we investigated the cellular uptake pathways and subcellular distribution of cRGD-Lipo@Ce6/DOX. Our studies revealed that low temperature (4 °C) completely blocked the uptake of cRGD-Lipo@Ce6/DOX by Hep G2 and Huh 7 cells, indicating that the liposomes enter cells via an energy-dependent endocytosis pathway (Figure 3A). Additionally, the use of CPZ (a clathrin-mediated endocytosis inhibitor), EIPA (a macropinocytosis receptor inhibitor), and Filipin (a caveolae-mediated endocytosis inhibitor) did not impact the internalization of cRGD-Lipo@Ce6/DOX (Figure 3A). Furthermore, cRGD-Lipo @Ce6/DOX (red and yellow lines) consistently colocalized with lysosomes (green lines) at various incubation times

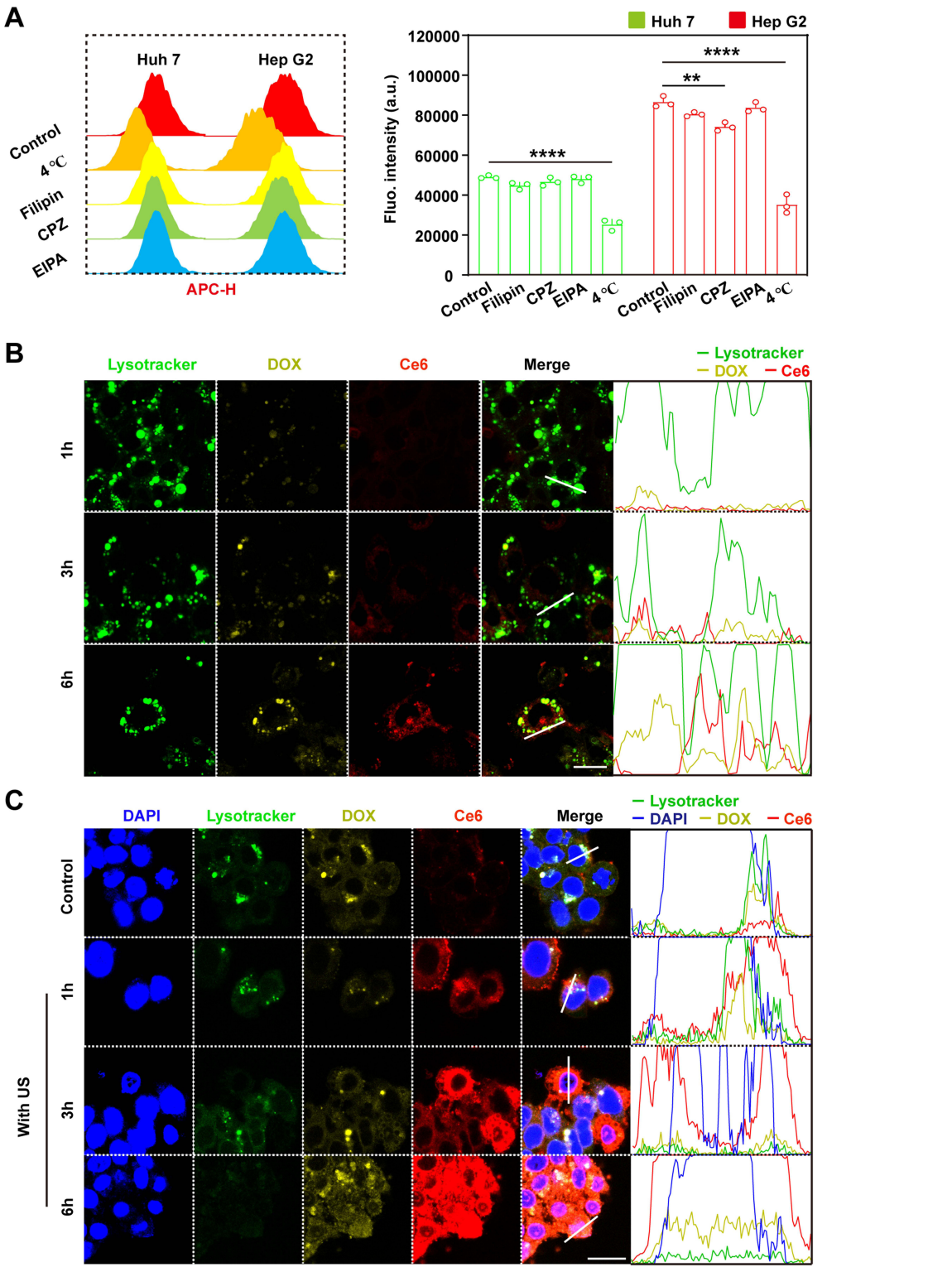


**Figure 3** Endocytosis pathway and intracellular distribution of cRGD-Lipo@Ce6. (**A**) Flow cytometry was performed using the APC fluorescence channel to examine the uptake of cRGD-Lipo@Ce6 by Hep G2 and Huh 7 cells. The cells were treated with various inhibitors and energy inhibitors (4 °C) for 1 hour. The conditions included cRGD-Lipo@Ce6 at 2 μg $mL^{-1}$ Ce6, and the inhibitors CPZ (30 μM), Filipin (7.5 μM), and EIPA (20 μM). $^{**}p < 0.01$ and $^{****}p < 0.0001$. (**B**) CLSM was used to observe cRGD-Lipo@Ce6/DOX in Hep G2 cells after incubation for 1, 3, and 6 hours (left). Lysotracker (green) was used to label lysosomes, and Hoechst 33342 (blue) was used to label nuclei. The intracellular fluorescence intensity of cRGD-Lipo@Ce6/DOX along the white line was analyzed using ImageJ (right). The formulation included 1 μg $mL^{-1}$ Ce6 and 2 μM DOX. (**C**) cRGD-Lipo@Ce6/DOX was incubated with Hep G2 cells for 2 hours, with or without US treatment, and then further incubated with the drugs for 1, 3, and 6 hours (left). Lysotracker (green) labeled lysosomes, and Hoechst 33342 (blue) labeled nuclei. The intracellular fluorescence intensity of cRGD-Lipo@Ce6/DOX (1 μg $mL^{-1}$ Ce6 and 2 μM DOX) along the white line was analyzed with ImageJ (right). US conditions: 80% duty cycle, 3 minutes. Scale bar: 20 μm.


https://doi.org/10.2147/IJN.S509387

(Figure 3B and Supplementary Figure 4A). Subsequently, we examined the intracellular drug release mechanism of cRGD-Lipo@Ce6/DOX. DiI (10 μM) was used to label membrane phospholipids to determine if cRGD-Lipo@Ce6/DOX underwent intracellular degradation by lysosomal hydrolases. Despite prolonged incubation, the fluorescence of DiI-labeled cRGD-Lipo@Ce6/DOX remained stable and was confined to lysosomes stained with LysoTracker green (Supplementary Figure 5). Thus, the drug release behavior of cRGD-Lipo@Ce6/DOX is minimally influenced by lysosomal hydrolysis during the observation period. These findings strongly suggest that cRGD-Lipo@Ce6/DOX primarily enters cells via the clathrin-mediated endocytosis pathway and that its distribution within the cell is closely associated with lysosomes, with minimal spontaneous lysosomal escape. Additionally, the stability of LNPs is maintained, likely due to the cholesterol in the membrane inhibiting phospholipase activity in lysosomes.[28]

Since lysosomal escape is a significant challenge in the development of LNP therapeutics, we aimed to facilitate the release of nanoparticles into the cytoplasm in a manner analogous to PCI.[29,30] Initially, we characterized apoptosis under various US parameters using flow cytometry and optimized these conditions (Supplementary Figure 6). Subsequently, we analyzed the subcellular distribution of cRGD-Lipo@Ce6/DOX before and after US activation. At different time points following US exposure, we observed that cRGD-Lipo@Ce6/DOX (red and yellow) gradually diffused from lysosomes (green) into the cytoplasm. In contrast, in the non-US group, the nanoparticles remained predominantly within the lysosomes. Additionally, the fluorescence quenching of DOX and Ce6, caused by tight encapsulation within the lipid structure, was partially alleviated following US treatment, indicating potential drug release (Figure 3C and Supplementary Figure 4B).[31] It is worth noting that as the incubation time is extended, the entry of drugs into the cytoplasm gradually increases, while the lysosomal fluorescence further declines. This phenomenon may be attributed to the destruction of lysosomal integrity, which facilitates the release of drugs from lysosomes into the cytoplasm.

We used LAMP1 and DCFH-DA to investigate whether the lysosomal escape of cRGD-Lipo@Ce6/DOX after US was due to the rapid cleavage of the lysosomal membrane by ROS produced by SDT or the diffusion of small molecule drugs through pores in the lysosomal membrane.[32] In each treatment group of Hep G2 and Huh 7 cells, cells treated with cRGD-Lipo@Ce6 + US alone showed increased ROS stained with DCFH-DA (green) and decreased lysosomes stained with LysoTracker (red) (Figure 4A and Supplementary Figure 7). LAMP1, a lysosomal membrane protein labeled with a green fluorescent secondary antibody, showed a significant decrease in fluorescence only in the cRGD-Lipo@Ce6 + US group, indicating damage to lysosomal membrane integrity (Figure 4B). In summary, the ROS generated by SDT not only accelerate drug release but also facilitate lysosomal escape by compromising lysosomal membrane integrity.

## cRGD-Lipo@Ce6/DOX Can Induce Effective Combination Therapies in Vitro

The biosafety of cRGD-Lipo@Ce6/DOX was initially assessed using the standard CCK-8 assay. After incubating the cRGD-Lipo@Ce6 with HHL-5, Huh 7, and Hep G2 cells for 24 hours, cell viability at each Ce6 concentration (0.5, 1, 2, 5 μg $mL^{-1}$) was significantly higher than that of the Free Ce6 group at the same concentrations. This indicates that the nanosystems have relatively good biosafety (Supplementary Figure 8).

Firstly, we quantified the levels of ROS production in each group using flow cytometry. Given that nanosystems (cRGD-Lipo) were employed to enhance drug internalization efficiency, the ROS generated by US excitation in the cRGD-Lipo@Ce6 group were 1.84 times higher than those in the Free Ce6 group (Supplementary Figure 9). Subsequently, the combined therapeutic efficacy of the cRGD-Lipo@Ce6/DOX on Hep G2 and Huh 7 cells were evaluated by examining cell cycle distribution and cell viability following various treatments. PI staining was used to assess the effects of DOX released from cRGD-Lipo@Ce6/DOX on the cell cycle of Hep G2 cells, and flow cytometry was employed for analysis. In the control group, no significant changes in cell cycle distribution were observed between cRGD-Lipo@Ce6 and the control group, indicating that US and ROS alone did not affect the cell cycle (Figure 5). Similarly, no significant changes in the cell cycle were noted in the cRGD-Lipo@Ce6/DOX group, possibly due to the high stability of the liposomes preventing early release of DOX. However, in the cRGD-Lipo@Ce6/DOX + US-treated Hep G2 cells, the proportion of cells in the G1 phase decreased by 58.33%, while the proportion in the S phase increased by 58.19% (Figure 5). In summary, DOX released by the cRGD-Lipo @Ce6/DOX + US group can induce cell cycle arrest in the S phase, consistent with the effects of free DOX, leading to increased cancer cell death. The apoptosis of Hep G2 and Huh 7 cells treated with SDT combined with DOX was evaluated using flow cytometry. Cytotoxicity in the untreated groups remained almost negligible (>95%) throughout the observation

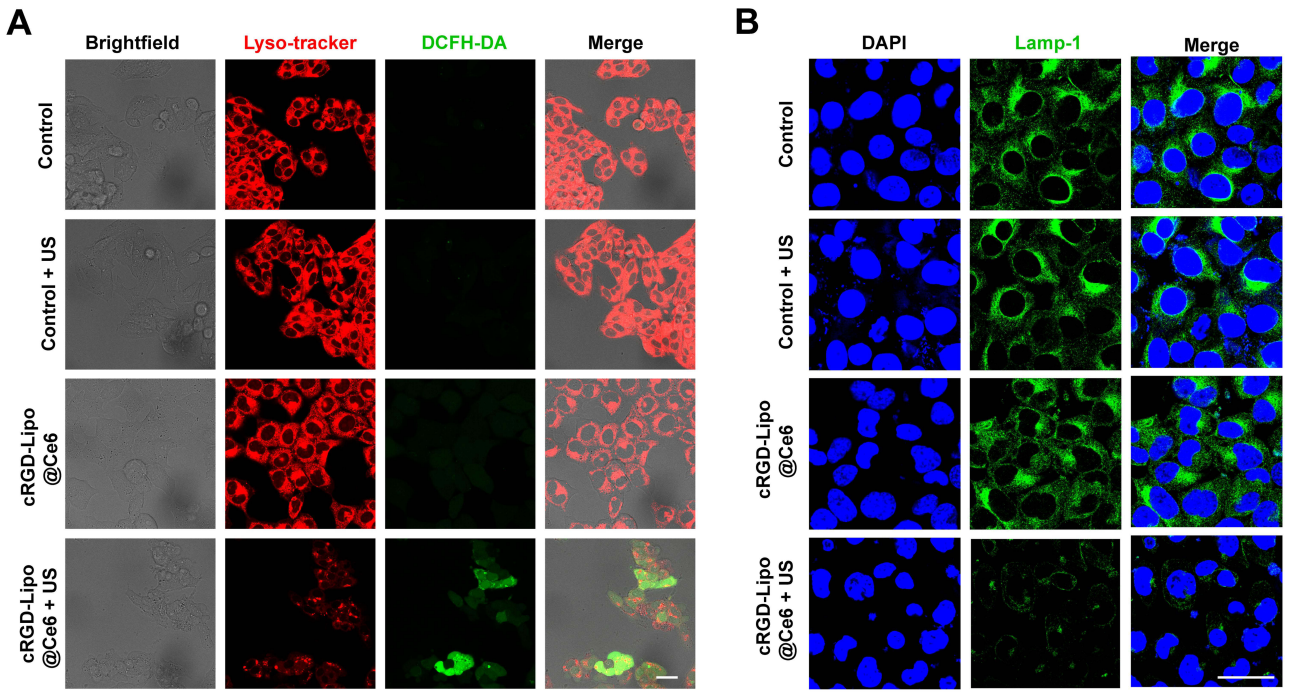


**Figure 4** Damage of Hep G2 lysosomes by SDT. (**A**) CLSM images of Hep G2 cells incubated for 6 hours with PBS or cRGD-Lipo@Ce6 and treated with or without US. Intracellular ROS was labeled with DCFH-DA (green), and lysosomes were labeled with LysoTracker (red). cRGD-Lipo@Ce6 (2 μg $mL^{-1}$ Ce6). US conditions were 80% duty cycle for 3 minutes. (**B**) CLSM images of Hep G2 cells incubated for 2 hours with PBS or cRGD-Lipo@Ce6 and treated with or without US. LAMP1 was labeled with a 488-FL secondary antibody (green), and the nucleus was labeled with Hoechst 33342 (blue). cRGD-Lipo@Ce6 (2 μg $mL^{-1}$ Ce6); US conditions were 80% duty cycle for 3 minutes. Scale bar: 25 μm.

period (Figure 6A and B). After ultrasound treatment (80% duty cycle, 5 minutes), no significant cytotoxicity was observed in the control group, indicating that ultrasound alone does not have a critical role in tumor therapy. The cytotoxicity of the cRGD-Lipo@Ce6 + US group was significantly higher than that of the Free Ce6 + US group, likely due to the lower uptake efficiency of free Ce6 by Hep G2 and Huh 7 cells (Figure 6A and B). Moreover, the apoptosis level induced by the DOX + US combined therapy was significantly higher (43% for Hep G2 and 51% for Huh 7) compared to the DOX (15% for Hep G2 and 15% for Huh 7) and cRGD-Lipo@Ce6 + US (28% for Hep G2 and 30% for Huh 7) groups (Figure 6A and B). These findings strongly suggest that cRGD-Lipo@Ce6/DOX have high biosafety and efficacy as combination therapies.

## In Vivo Antitumor Treatment

Most nanomedicine delivery to the tumor site via intravenous injection is inefficient, often resulting in poor bioavailability and limited therapeutic efficacy.[33,34] Therefore, we chose local administration (intratumoral injection) as an alternative approach, which can significantly improve drug bioavailability and enhance therapeutic outcomes. In fact, intratumoral injection as a viable alternative to systemic therapy, especially in advanced HCC.[7] First, we evaluated the impact of RGD peptide modification on drug delivery efficiency through intratumoral injection, using tumor fluorescence imaging for comparison. Tumor fluorescence imaging conducted 6 hours after intratumoral injection revealed that the average fluorescence intensity of the RGD peptide-modified group was significantly higher than that of the unmodified group (Supplementary Figure 10). This indicates that the modification with RGD peptide effectively enhanced the accumulation of drugs in tumor tissues. Therefore, cRGD-Lipo@Ce6/DOX was selected as the representative formulation with the greatest potential for in vivo applications, and its biological distribution in mice were evaluated. Following intratumoral injection of the drug, in vitro fluorescence imaging of tumors at different time points revealed the highest drug accumulation at 6 hours post-injection (Supplementary Figure 11). The accumulation of drugs in the liver progressively increases and reaches its peak at 12 hours, followed by a significant decline at 24 hours. This trend is likely attributed to that nanomedical drugs with a size of 100 nm are primarily metabolized by the liver (Supplementary Figure 12).


https://doi.org/10.2147/IJN.S509387

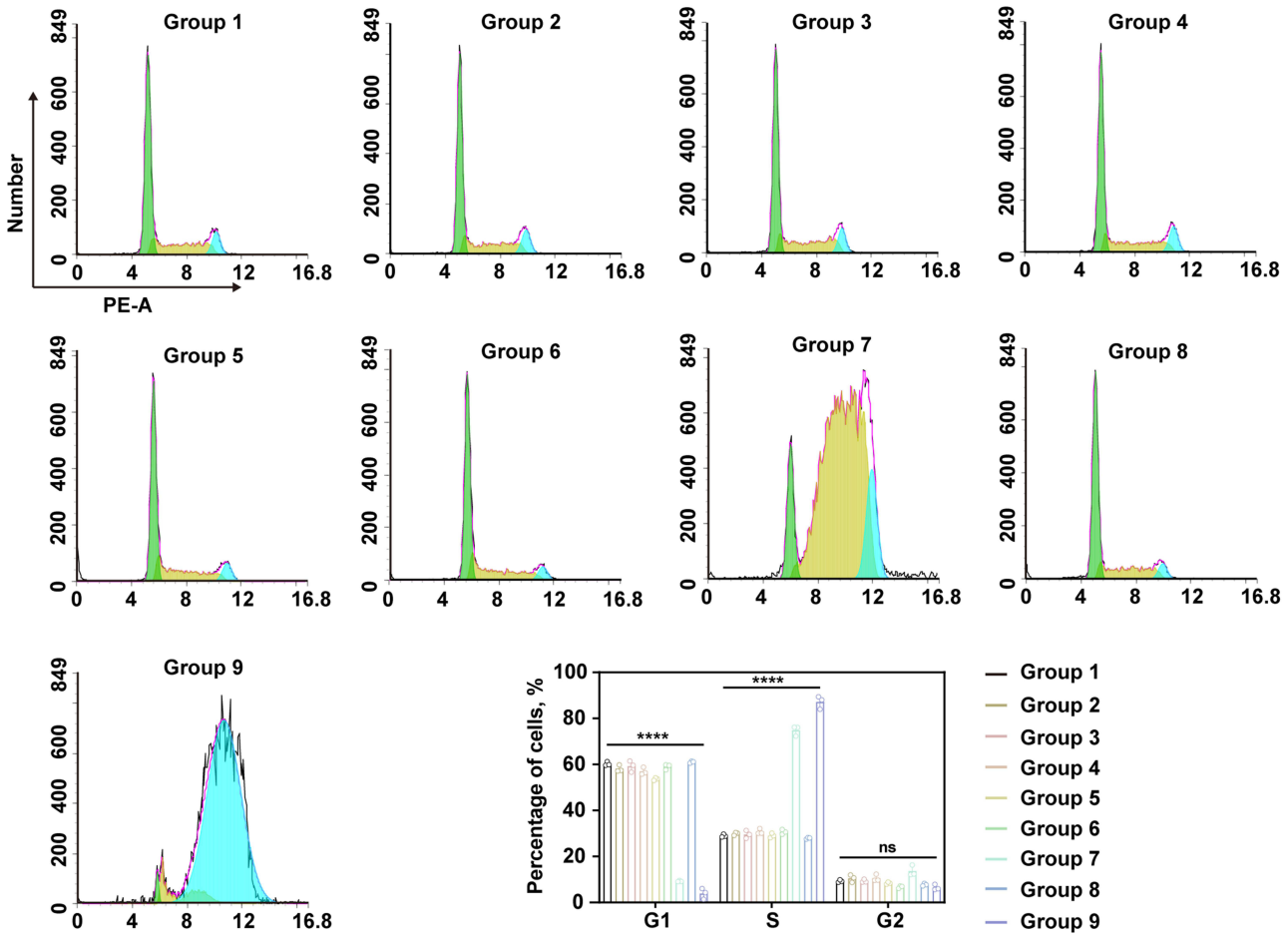


**Figure 5** The cell cycle levels of Hep G2 cells were analyzed by flow cytometry after 30 minutes of staining with PI at room temperature. Group 1–9 represented 1: control, 2: control + US, 3: Free Ce6, 4: Free Ce6 + US, 5: cRGD-Lipo@Ce6, 6: cRGD-Lipo@Ce6 + US, 7: Free DOX, 8: cRGD-Lipo@Ce6/DOX, and 9: cRGD-Lipo@Ce6/DOX + US. Ce6 was used at a concentration of 1 μg $mL^{-1}$, and DOX was used at a concentration of 2 μM. US was applied with an 80% duty cycle for 5 minutes. ****$p < 0.0001$.

The anticancer activity of SDT combined with chemotherapy was investigated in Huh 7 subcutaneous tumor-bearing mice. When the implanted tumors reached ~150 $mm^3$ (day 7), the mice were treated with various regimens via intratumoral injection. The treatment groups included: PBS, cRGD-Lipo@Ce6, cRGD-Lipo@Ce6 + US, cRGD-Lipo @Ce6/DOX, DOX, or cRGD-Lipo@Ce6/DOX + US. Given the excellent drug accumulation observed in the tumor after 6 hours of treatment, we ultimately decided to perform US stimulation at the 6-hour mark following intratumoral drug injection (Supplementary Figure 12). Measure and record tumor volume (V) every other day during treatment. All treatment groups were killed at the end of treatment (day 15), and the tumors were collected for further analysis (Figure 7A–F). The antitumor efficacy of combining SDT with chemotherapy was assessed using Huh 7 tumor-bearing mouse models (Figure 7A). The tumor volume measurements revealed that the cRGD-Lipo@Ce6 + US group had a significantly reduced tumor volume (406.53 ± 150.56 $mm^3$) compared to the control group (PBS), which had a tumor volume of 788.32 ± 135.62 $mm^3$ (Figure 7B and C). This indicates that SDT alone is effectively inhibited tumor growth. However, when compared to the DOX group (373.64 ± 26.31 $mm^3$), the tumor inhibition effect of the cRGD-Lipo@Ce6/DOX group (549.92 ± 41.62 $mm^3$) did not show a significant improvement. This may be attributed to the limited efficacy of the slow, sustained drug release on tumor suppression in vivo. The highest tumor inhibition was observed in the cRGD-Lipo@Ce6/DOX + US group, with a tumor volume of 69.92 ± 17.17 $mm^3$, which was significantly superior to both the DOX group and the cRGD-Lipo@Ce6 + US group. Thus, it can be concluded that among the six treatment modalities evaluated, the combination of SDT and chemotherapy is the most effective, achieving a final tumor inhibition rate of 94% (Supplementary Figure 13).

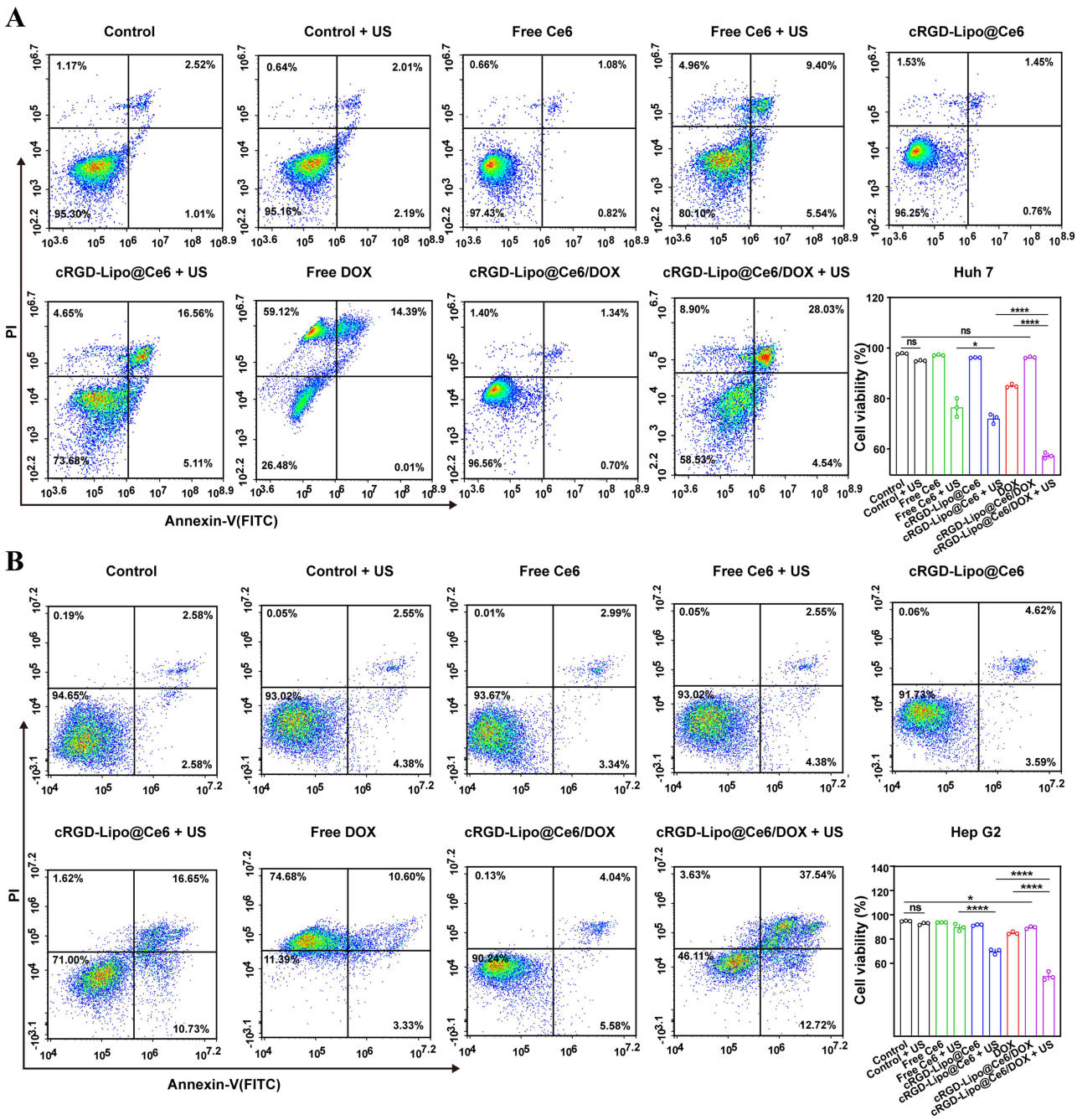


**Figure 6** Apoptotic levels of Huh 7 cells (**A**) and Hep G2 cells (**B**) were assessed by flow cytometry after staining with membrane connexin V-FITC and PI at room temperature for 15 minutes. The treatments included: control, control + US, Free Ce6, Free Ce6 + US, cRGD-Lipo@Ce6, cRGD-Lipo@Ce6 + US, Free DOX, cRGD-Lipo @Ce6/DOX, and cRGD-Lipo@Ce6/DOX + US. Ce6 was used at a concentration of 2 μg $mL^{-1}$, and DOX was used at 4 μM. US was applied with an 80% duty cycle for 5 minutes. *$p < 0.05$ and ****$p < 0.0001$.

The body weight of mice in each group was recorded through observation. No significant difference in weight distribution was observed between each treatment group and the control group (PBS) (Figure 7D). This could be attributed to the high safety profile of the dual-modality therapy and ultrasound parameters used. Additionally, the varying weights of subcutaneous tumors among the groups might also contribute to this observation. The biosafety of each treatment group was further evaluated using histological evaluation, as well as through tests of liver and kidney function. Histological evaluation via H&E staining demonstrated that in each treatment group, cardiomyocytes exhibited intact muscle fibers, with no evidence of significant inflammatory infiltration or necrosis (Figure 7E). Hepatocytes


https://doi.org/10.2147/IJN.S509387

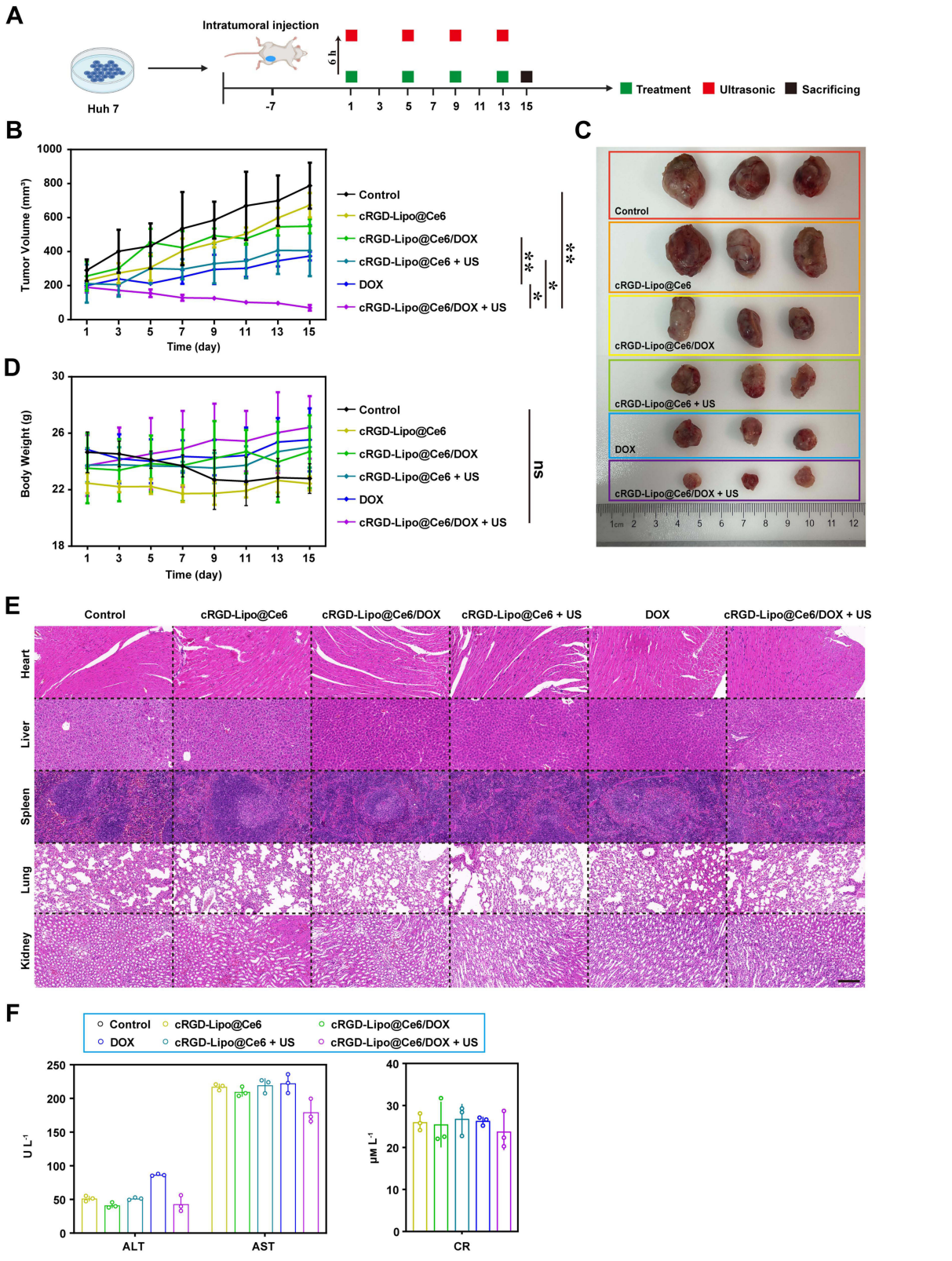


**Figure 7** In vivo tumor therapy. (**A**) Huh 7 tumor-bearing mice were treated with intratumoral injection and then stimulated with ultrasound 6 hours later, included PBS, cRGD-Lipo@Ce6, cRGD-Lipo@Ce6/DOX, cRGD-Lipo@Ce6 + US, DOX or cRGD-Lipo@Ce6/DOX + US. Measured and recorded: (**B**) mouse tumor volume, (**C**) picture of isolated tumor, and (D) mouse weight. After treatment, (**E**) perform pathological analysis of the five normal viscera in each treatment, (**F**) and to serum from mice group was collected to assess liver and kidney function. Ce6 (10 mg $kg^{-1}$) and DOX (6.4 mg $kg^{-1}$). US condition: 80% duty, 5 minutes. Scale bar = 200 μm. *$p < 0.05$ and **$p < 0.01$.

maintained a complete structural integrity, and no obvious hemorrhagic necrosis was observed. The spleen and lung tissues appeared intact, with no apparent inflammatory cell infiltration. Additionally, the renal tubular epithelial cells in the kidneys showed no signs of degeneration or edema. The results indicated that the activities of ALT, AST, and CR were all within the normal reference range (Figure 7F). This suggests that liver and kidney functions were normal, with no obvious signs of damage.

## Conclusion

In summary, we developed a cooperative DDS using liposomes loaded with chemotherapy drugs and sonosensitizers. We utilized EDC/NHS-mediated bio-coupling technology to modify the surface with c(RGDyK) for targeted enrichment and enhanced tumor infiltration at HCC sites. In vitro experiments demonstrated that cRGD-Lipo@Ce6/DOX effectively achieves controlled drug release and lysosomal escape under local US guidance. In vivo anti-tumor studies revealed that cRGD-Lipo@Ce6/DOX exhibits high biological safety and exceptional anti-tumor efficacy, with an inhibition rate of 94%. This study introduces a simple, safe, and efficient method for controlled drug release and promoting the lysosomal escape of drug-carrying liposomes through the activation of sonodynamic drugs using US. Therefore, this combination therapy, based on ultrasound-controlled SDT and chemotherapy, shows significant potential and provides additional treatment options for patients with advanced HCC. Nevertheless, several key challenges remain unresolved. These include optimizing the biocompatibility of sonodynamic liposomes and understanding their potential impact on the immune system. Moreover, studies have demonstrated that passive diffusion drug delivery systems, including liposomes, which rely on the enhanced permeability and retention (EPR) effect, are inefficient for targeted tumor cells. This inefficiency restricts their broader clinical application. Consequently, the development of liposome-based drug delivery systems with enhanced selectivity and delivery efficiency represents a crucial direction for future research.

## Data Sharing Statement

The data supporting the findings of this study are available upon request from the corresponding author. Due to privacy or ethical restrictions, the data are not publicly accessible. This version maintains clarity and conciseness while emphasizing the reasons for data restriction.

## Acknowledgments

This research was funded by National Nature Science Foundation of China (grant number: 81271677), Medical Science and Technology Project of Zhejiang Province (grant number: 2024KY011).

## Disclosure

The authors declare no conflicts of interest in this work.

## References

1. Laversanne M BF, Sung H, Sung H, et al. Global cancer statistics 2022: GLOBOCAN estimates of incidence and mortality worldwide for 36 cancers in 185 countries. *CA Cancer J Clin*. 2024;74:229–263. doi:10.3322/caac.21834
2. Singal A, Kanwal F, Llovet J. Global trends in hepatocellular carcinoma epidemiology: implications for screening, prevention and therapy. *Nat Rev Clin Oncol*. 2023;20:864–884. doi:10.1038/s41571-023-00825-3
3. Yang C, Zhang H, Zhang L, et al. Evolving therapeutic landscape of advanced hepatocellular carcinoma. *Nat Rev Gastroenterol Hepatol*. 2023;20:203–222. doi:10.1038/s41575-022-00704-9
4. Carvalho C, Santos R, Cardoso S, et al. Doxorubicin: the good, the bad and the ugly effect. *Curr Med Chem*. 2009;16:3267–3285. doi:10.2174/092986709788803312
5. Finn R, Qin S, Ikeda M, et al. Atezolizumab plus Bevacizumab in unresectable hepatocellular carcinoma. *N Engl J Med*. 2020;382:1894–1905. doi:10.1056/NEJMoa1915745
6. Cheng A, Qin S, Ikeda M, et al. Updated efficacy and safety data from IMbrave150: atezolizumab plus bevacizumab vs. sorafenib for unresectable hepatocellular carcinoma. *J Hepatol*. 2022;76:862–873. doi:10.1016/j.jhep.2021.11.030
7. Cappuyns S, Corbett V, Yarchoan M, et al. Critical appraisal of guideline recommendations on systemic therapies for advanced hepatocellular carcinoma: a review. *JAMA Oncol*. 2024;10:395–404. doi:10.1001/jamaoncol.2023.2677
8. Zhou X, Yao Z, Bai H, et al. Treatment-related adverse events of PD-1 and PD-L1 inhibitor-based combination therapies in clinical trials: a systematic review and meta-analysis. *Lancet Oncol*. 2021;22:1265–1274. doi:10.1016/S1470-2045(21)00333-8

9. Bruix J, Qin S, Merle P, et al. Regorafenib for patients with hepatocellular carcinoma who progressed on sorafenib treatment (RESORCE): a randomised, double-blind, placebo-controlled, Phase 3 trial. *Lancet*. 2017;389:56–66. doi:10.1016/S0140-6736(16)32453-9
10. Abou-Alfa G, Meyer T, Cheng A, et al. Cabozantinib in patients with advanced and progressing hepatocellular carcinoma. *N Engl J Med*. 2018;379:54–63. doi:10.1056/NEJMoa1717002
11. Liang S, Deng X, Ma P, et al. Recent advances in nanomaterial-assisted combinational sonodynamic cancer therapy. *Adv Mater*. 2020;32:e2003214. doi:10.1002/adma.202003214
12. Ruoslahti E, Pierschbacher MD. New perspectives in cell adhesion: RGD and integrins. *Science*. 1987;238:491–497. doi:10.1126/science.2821619
13. Shang Y, Zhang H, Cheng Y, et al. Fluorescent imaging-guided chemo- and photodynamic therapy of hepatocellular carcinoma with HCPT@NMOFs-RGD nanocomposites. *Int J Nanomed*. 2022;17:1381–1395. doi:10.2147/IJN.S353803
14. Xu J, Zheng Q, Cheng X, et al. Chemo-photodynamic therapy with light-triggered disassembly of theranostic nanoplatform in combination with checkpoint blockade for immunotherapy of hepatocellular carcinoma. *J Nanobiotechnol*. 2021;19:355–375. doi:10.1186/s12951-021-01101-1
15. Li Z, Zhang H, Han J, et al. Surface nanopore engineering of 2D MXenes for targeted and synergistic multitherapies of hepatocellular carcinoma. *Adv Mater*. 2018;30:e1706981. doi:10.1002/adma.201706981
16. Tu L, Liao Z, Luo Z, et al. Ultrasound-controlled drug release and drug activation for cancer therapy. *Exploration*. 2021;1:20210023. doi:10.1002/EXP.20210023
17. Banushi B, Joseph S, Lum B, et al. Endocytosis in cancer and cancer therapy. *Nat Rev Cancer*. 2023;23:450–473. doi:10.1038/s41568-023-00574-6
18. Madsen S, Gonzales J, Zamora G, et al. Comparing the effects of light- or sonic-activated drug delivery: photochemical/sonochemical internalization. *J Environ Pathol Toxicol Oncol*. 2016;35(1):91–98. doi:10.1615/JEnvironPatholToxicolOncol.2016015463
19. Barenholz Y. Doxil®–the first FDA-approved nano-drug: lessons learned. *J Control Release*. 2012;160:117–134. doi:10.1016/j.jconrel.2012.03.020
20. Chatterjee S, Kon E, Sharma P, et al. Endosomal escape: a bottleneck for LNP-mediated therapeutics. *Proc Natl Acad Sci U S A*. 2024;121:e2307800120. doi:10.1073/pnas.2307800120
21. Xu X, Tian F, Pan Y, et al. Emerging mechanistic insights into liposomal stability: full process management from production and storage to food application. *Chem Eng J*. 2025;505:159552. doi:10.1016/j.cej.2025.159552
22. Yu L, Wang Z, Mo Z, et al. Synergetic delivery of triptolide and Ce6 with light-activatable liposomes for efficient hepatocellular carcinoma therapy. *Acta Pharm Sin B*. 2021;11:2004–2015. doi:10.1016/j.apsb.2021.02.001
23. Kim B, Han G, Toley BJ, et al. Tuning payload delivery in tumour cylindroids using gold nanoparticles. *Nat Nanotechnol*. 2010;5:465–472. doi:10.1038/nnano.2010.58
24. Zhang P, Zhang H, Zheng B, et al. Combined self-assembled hendeca-arginine nanocarriers for effective targeted gene delivery to bladder cancer. *Int J Nanomed*. 2022;17:4433–4448. doi:10.2147/IJN.S379356
25. Zheng B, Liu Z, Wang H, et al. R11 modified tumor cell membrane nanovesicle-camouflaged nanoparticles with enhanced targeting and mucus-penetrating efficiency for intravesical chemotherapy for bladder cancer. *J Control Release*. 2022;351:834–846. doi:10.1016/j.jconrel.2022.09.055
26. Huo S, Ma H, Huang K, et al. Superior penetration and retention behavior of 50 nm gold nanoparticles in tumors. *Cancer Res*. 2013;73:319–330. doi:10.1158/0008-5472.CAN-12-2071
27. Lange K. Food science and COVID-19. *Food Sci Hum Wellness*. 2021;10:1–5. doi:10.1016/j.fshw.2020.08.005
28. Mouritsen OG, Jørgensen K. A new look at lipid-membrane structure in relation to drug research. *Pharm Res*. 1998;15:1507–1519. doi:10.1023/A:1011986613392
29. Filipczak N, Pan J, Yalamarty SSK, Torchilin VP. Recent advancements in liposome technology. *Adv Drug Deliv Rev*. 2020;156:4–22. doi:10.1016/j.addr.2020.06.022
30. Yin H, Sun L, Pu Y, et al. Ultrasound-controlled CRISPR/Cas9 system augments sonodynamic therapy of hepatocellular carcinoma. *ACS Cent Sci*. 2021;7:2049–2062. doi:10.1021/acscentsci.1c01143
31. Huang J, Xiao Z, An Y, et al. Nanodrug with dual-sensitivity to tumor microenvironment for immuno-sonodynamic anti-cancer therapy. *Biomaterials*. 2021;269:120636. doi:10.1016/j.biomaterials.2020.120636
32. Vanwalleghem G, Fontaine F, Lecordier L, et al. Coupling of lysosomal and mitochondrial membrane permeabilization in trypanolysis by APOL1. *Nat Commun*. 2015;6:8078. doi:10.1038/ncomms9078
33. Wilhelm S, Tavares A, Dai Q, et al. Analysis of nanoparticle delivery to tumours. *Nat Rev Mater*. 2016;1:16014. doi:10.1038/natrevmats.2016.14
34. Sindhwani S, Syed A, Ngai J, et al. The entry of nanoparticles into solid tumours. *Nat Mater*. 2020;19:566–575. doi:10.1038/s41563-019-0566-2